Nanomechanical displacement detection using coherent transport in graphene nanoribbon resonators

A. Isacsson[*]

Department of Applied Physics, Chalmers University of Technology, SE-412 96 Göteborg, Sweden
(Received 30 June 2011; published 30 September 2011)

Graphene nanoribbons provide an opportunity to integrate phase-coherent transport phenomena with nanoelectromechanical systems (NEMS). Due to the strain induced by a deflection in a graphene nanoribbon resonator, coherent electron transport and mechanical deformations couple. This coupling can be used for sensitive displacement detection in both armchair and zigzag graphene nanoribbon NEMS. Here it is shown that for ordered as well as disordered ribbon systems of length L, a strain $\epsilon \sim (w/L)^2$ due to a deflection w leads to a relative change in conductance $\delta G/G \sim (w^2/a_0 L)$, where $a_0 \approx 1.4$ Å.

I. INTRODUCTION

Nanoelectromechanical (NEM) resonators[1] hold promise for technological implementations such as tunable rf filters[2] and ultrasensitive mass sensing.[3,4] NEMS are also of interest in connection with fundamental studies of quantum properties of macroscopic systems.[5–7] Regardless of application area, transduction mechanisms for system control and readout must be implemented.[8] The choice of transduction mechanism depends, among other things, on device design and choice of material.

Being only a single atomic layer thick, graphene constitutes the ultimate material for two-dimensional NEMS, and graphene NEMS have already been demonstrated.[9–16] The transduction schemes used so far have been optical,[9,11,12] mechanical,[10] and electric.[13–16] Because electron transport through mesoscopic graphene devices can be coherent,[17–19] using graphene in NEMS means that phase coherent transport phenomena can be directly integrated into NEM resonators. As shown in this paper, this allows the motion of the NEMS to couple to the length scale set by an intrinsic scale, the interatomic distance $a_0 \approx 1.4$ Å.

So far graphene NEMS have operated in the diffusive transport regime where electric transduction[13–16] has been based on charge carrier density modulation. In those experiments the graphene was suspended above a backgate at distance d as shown in Fig. 1(a). For a sheet of length L and width W the capacitance to the gate can be estimated as $C_G \approx \varepsilon_0 L W / d$, where ε_0 is the vacuum permittivity.[20,21] Hence the backgate voltage V_G induces a carrier density $n_0 e = \varepsilon_0 V_G / d$. This leads to a conductivity of $\sigma = \mu_e \varepsilon_0 V_G / d$,[22] where μ_e is the electron mobility. Motion detection then uses the change in carrier density with distance. For a deflection w away from the equilibrium distance d, the relative change in conductivity is $\delta\sigma/\sigma \sim w/d$.[23] Note that only geometric length scales (w and d) enter into this expression.

A deflection w also induces strain $\epsilon \approx (w/L)^2$, which affects both the dynamical[13,24] and the electronic[25] properties. For diffusive transport, strain leads to a linear increase in resistance[26] with a constant of proportionality of order unity. Hence the relative change in conductivity due to strain, $\delta\sigma_{\text{strain}}/\sigma \sim (w/L)^2$, is typically negligible compared to that from the carrier density modulation. For ballistic transport in wide sheets, similar conclusions hold (see Ref. 23).

The situation is different if one considers coherent transport in graphene nanoribbons. The transverse confinement then gives rise to conductance quantization.[27,28] On a plateau of constant conductance, this prevents changes of conductivity due to motion in the backgate electrostatic field, leaving strain as the dominant coupling between deformation and conductance. Recently, conductance quantization in ballistic suspended graphene samples was demonstrated.[29] In this paper it is shown that in graphene nanoribbon NEM devices, an operating point where σ changes with displacement as $\delta\sigma/\sigma = \delta\sigma_{\text{strain}}/\sigma \sim (w^2/a_0 L)$ can be found. For armchair nanoribbons [Fig. 1(b)], this is due to the opening of the transport gap. For zigzag nanoribbons, which has no transport gap, an interferometer-type setup [Fig. 1(c)] can be used. This setup can also be used in the presence of edge disorder.

Typically, graphene NEMS in equilibrium is not under zero strain. Not only will this inhibit ripple formation, it will also lead to more linear mechanical response. This strain is typically due to built-in strain or to biasing to a working point w_0. For the cases studied here, it is shown that biasing to the working point will not create any appreciable strain and only built-in strain needs to be considered.

Transport through suspended graphene sheets and ribbons and in graphene with strained regions has been studied previously by several researchers,[30–33] as well as in carbon nanotubes.[34,35] The prospects of using strain in a controlled way to influence electronic properties is currently an active research field. Here the focus is on displacement detection in graphene nanoribbon NEMS.

This paper is organized as follows: In Sec. II the tight binding model for uniaxially strained graphene is briefly reviewed. Then, in Sec. III the sensitivity to deflections of an armchair nanoribbon [Fig. 1(b)] is considered, while Sec. IV treats the interferometric setup using zigzag nanoribbons [Fig. 1(c)]. Conclusions are found in Sec. V.

II. TIGHT BINDING DESCRIPTION

The electronic properties close to the charge neutrality point are to a first approximation well described by the nearest
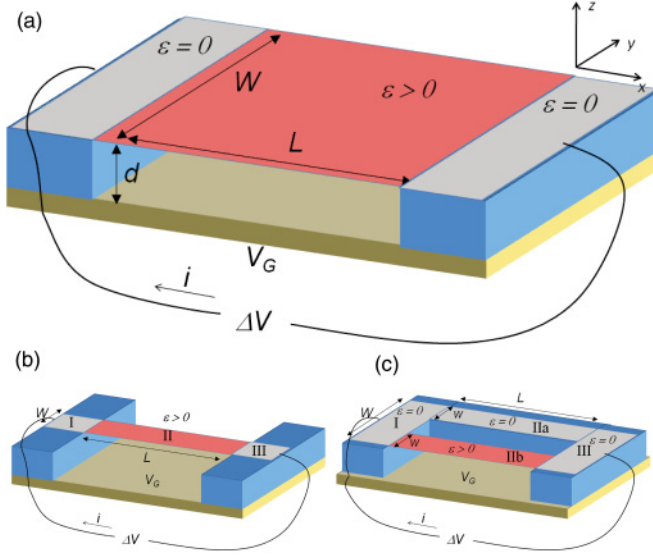
FIG. 1. (Color online) Suspended graphene NEM systems. (a) Graphene sheet of length L and width W suspended in the xy plane above a backgate. (b) Single suspended nanoribbon. For armchair nanoribbons, the strain induces a transport gap which can be used for displacement detection. (c) Graphene nanoribbon interferometer for displacement detection using zigzag nanoribbons.

neighbor tight binding model. Suppressing spin indices it is

$$H = -\sum_{n,\delta_i}\left[t_{n\delta_i}a_n^\dagger b_{n\delta_i} + \text{h.c.}\right] + \sum_m\left[V_m^{(a)}n_m^{(a)} + V_m^{(b)}n_{m\delta_1}^{(b)}\right].$$

(1)

Here $a_n^\dagger$ is the creation operator for an electron at the point $\mathbf{R}_n = (n_1\mathbf{a}_1 + n_2\mathbf{a}_2)$ and $b_{n\delta_i}$ the destruction operator for electrons at the site $\mathbf{R}_n + \delta_i$. The basis is here: $\mathbf{a}_1 = a_0(3/2,\sqrt{3}/2)$, $\mathbf{a}_2 = a_0(3/2, -\sqrt{3}/2)$, $\delta_1 = a_0(1/2,\sqrt{3}/2)$, $\delta_2 = a_0(1/2, -\sqrt{3}/2)$, and $\delta_3 = a_0(-1,0)$. For unstrained graphene, $t_{n\delta} = t_0 \approx 2.7$ eV, and the Fermi velocity is $\hbar v_F = 3t_0a_0/2$.

For uniform strain ϵ along the x direction (armchair edge), the bond lengths change from a_0 to

$$|\delta_1| = |\delta_2| = a_0[1 + 0.25\epsilon(1 - 3\sigma_p)],$$
$$|\delta_3| = a_0[1 + \epsilon], \qquad \text{(armchair)}$$

while for uniform strain in the y direction (zigzag edge),

$$|\delta_1| = |\delta_2| = a_0[1 + 0.25\epsilon(3 - \sigma_p)]$$
$$|\delta_3| = a_0[1 - \epsilon\sigma_p]. \qquad \text{(zigzag)}$$

Here $\sigma_p \approx 0.1$ is the Poisson ratio.

The changed lengths alter the hopping energies as $t_{n\delta_i} = t_0(1 + \Delta_i)$. Typically, $\epsilon \ll 1$ and it suffices to work to first order in ϵ. Then $\Delta_i \propto \epsilon$ and only first-order terms in Δ_i need to be kept. The spectrum then remains gapless and linear and can, for uniform strain, be described by the low-energy Hamiltonian $H = H_D + V$, where

$$H_D = \hbar v_F\begin{bmatrix} \hat{\Sigma}\cdot(-i\nabla + \mathbf{k}_0) & 0 \\ 0 & \hat{\Sigma}^*\cdot(-i\nabla - \mathbf{k}_0) \end{bmatrix}.$$

(2)

Here $\hat{\Sigma}$ is a modified $\hat{\sigma}$ matrix defined as

$$\hat{\Sigma} \equiv v_F^{-1}\begin{bmatrix} 0 & \mathbf{v} \\ \mathbf{v}^* & 0 \end{bmatrix} = v_F^{-1}\begin{bmatrix} 0 & v_x\hat{x} + v_y\hat{y} \\ v_x^*\hat{x} + v_y^*\hat{y} & 0 \end{bmatrix}, \quad (3)$$

where

$$\hbar v_x = \frac{3t_0a_0}{2}\left[1 + \frac{\Delta_1 + \Delta_2 + 4\Delta_3}{6} - i\frac{\sqrt{3}}{3}\frac{\Delta_1 - \Delta_2}{2}\right],$$
$$\hbar v_y = \frac{3t_0a_0}{2}\left[\frac{\Delta_1 - \Delta_2}{2\sqrt{3}} - i\left(1 + \frac{\Delta_1 + \Delta_2}{2}\right)\right],$$
$$\mathbf{k}_0 = \frac{1}{3a_0}(\sqrt{3}[\Delta_2 - \Delta_1], \Delta_1 + \Delta_2 - 2\Delta_3).$$

Hence the Fermi velocity changes and becomes anisotropic, and the locations of the Fermi points in wave-vector space changes.

The Δ_i values depend on the direction the strain is applied in and must be determined from first principles. In the context of carbon nanotubes, this has been studied extensively,[36–38] mainly using tight-binding Hückel theory or Koster-Slater calculations.[39] More recently, density functional theory has been applied to strained graphene.[40,41] Here, the model of Ribeiro *et al.*[41] is used, where $t_{\delta_i} = t_0 \exp[-\beta_i(\delta_i/a_0 - 1)]$.

For strain along the x direction (armchair) $\beta_1 = \beta_2 = 2.6$ and $\beta_3 = 3.3$,[41] and to lowest order in ϵ one finds

$$\hat{\Sigma} = (1 - 2.35\epsilon)\sigma_x\hat{x} + (1 - 0.46\epsilon)\sigma_y\hat{y}, \qquad (4)$$
$$\mathbf{k}_0 = \frac{2}{3a_0}2.84\epsilon\,\hat{y}. \qquad \text{(armchair)} \quad (5)$$

Here $\sigma_{x,y}$ are the conventional Pauli spin-1/2 matrices. For strain along the y direction (zigzag), $\beta_1 = \beta_2 = 3.15$ and $\beta_3 = 4$,[41] which gives

$$\hat{\Sigma} = (1 - 0.74\epsilon)\sigma_x\hat{x} + (1 - 2.30\epsilon)\sigma_y\hat{y}, \qquad (6)$$
$$\mathbf{k}_0 = -\frac{2}{3a_0}2.70\epsilon\,\hat{y}. \qquad \text{(zigzag)} \quad (7)$$

III. SUSPENDED ARMCHAIR RIBBON

Consider now the ideal situation with a perfect metallic armchair graphene nanoribbon of length L and width W, suspended above a backgate a distance d_0 as shown in Fig. 1(b). The supported parts (regions I and III) are assumed to be unstrained, while the suspended part (region II) is under under finite strain $\epsilon > 0$. For concreteness, consider the situation shown in Fig. 2. There it is assumed that the undeflected ($w = 0$) ribbon has a built-in strain ϵ_0 and an approximately uniform gate-induced charge density ρ_0.

The conductance through the ribbon in the linear response regime is proportional to the transmission function $T(E)$ as $G = 2(e/h^2)T(E)$, where the prefactor 2 accounts for spin. Confinement in the y direction leads to quantization of transverse wave-vector components, and if the ribbon were unable to deflect and was initially unstrained ($\epsilon_0 = 0$) the transmission $T(E)$ would show a steplike behavior with increasing E (see blue squares in Fig. 3).

The energy E can be controlled by the backgate which also changes the carrier density. For a narrow ribbon with $W/d \ll 1$ connected to a reservoir with chemical potential μ,
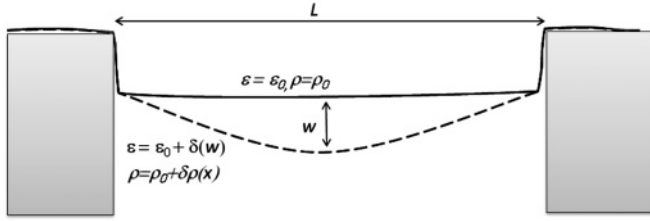
FIG. 2. Side view of suspended nanoribbon. In the text, a system where the ribbon is initially undeflected and has a finite induced 1D charge density ρ_0 and a built-in uniaxial strain ϵ_0. A deflection of magnitude w will induce an additional strain $\delta(w) \sim w^2/L^2$ as well as modify the charge distribution in the ribbon to $\rho = \rho_0 + \delta\rho(x)$.

one finds (see Appendix A), to leading order in d/W, that the correspondingly induced charge density is

$$\rho \approx \beta \frac{\mu}{1 + \alpha \ln \frac{8d}{W}}, \quad (8)$$

with $\alpha \equiv e^2/(3\pi^2 t_0 a_0 \varepsilon_0) \approx 1.6$ and $\beta = 4e/(3\pi t_0 a_0)$. Note that ε_0 denotes the vacuum permittivity while the symbol ϵ_0 denotes initial strain.

In what follows we will be mainly interested in one-dimensional (1D) charge densities ρ such that only the lowest transverse subband is occupied. This implies that the maximum 1D charge density is of the order $\rho \lesssim e/W$. If the ribbon is suspended, changing the charge density (bias voltage) may cause the ribbon to deflect.
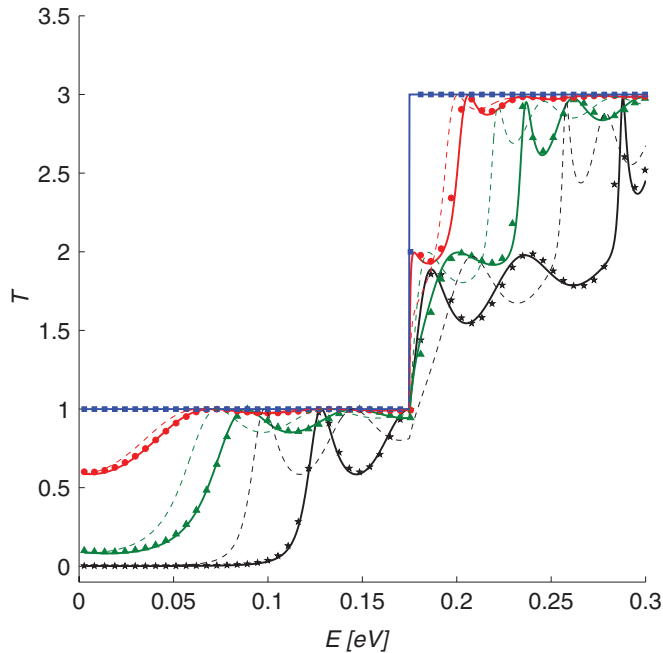

FIG. 3. (Color online) Transmission probability $\mathcal{T}$ through the metallic armchair ribbon ($W = 17$ nm, $L = 28$ nm) [see Fig. 1(b)] as a function of $\mathcal{E}$ and ϵ. The solid lines follow from the long wavelength approximation [Eq. (12)] for the strains $\epsilon = 0.0\%$ (blue squares), 0.2% (red circles), 0.5% (green triangles), and 1.0% (black stars). The discrete symbols were obtained using numerical tight-binding calculations. The thin dashed line corresponds to making the calculation in the absence of the deformation potential.

To see that one can tune ρ using the backgate without significantly affecting the deflection w of the ribbon, which is what one wishes to measure, consider the pressure induced on the ribbon. Using relation (8) one finds that for $\rho = \rho_{\text{max}} = e/W$ a maximum pressure of $P_z = e^2/(8\pi\varepsilon_0 W^3 d)$. Hence by choosing a large backgate distance d (or using a side gate to control ρ), this force can be made arbitrarily small while allowing the backgate to tune the charge density in the interval $0 < |\rho| < e/W$. An example calculation explicitly demonstrating this is found in Appendix B.

Note here that it is this weak dependence of the pressure P_z on the deflection w of the ribbon which allows one to assume that the strain in the ribbon will remain uniform throughout the ribbon at all times.

To calculate $T(E)$, the transverse momentum is divided into wave-vector components $q_n = 2\pi/3\sqrt{3}a_0 + n\pi/W + k_0$ for integer n. Here k_0 is given by Eq. (5). If the interfaces between strained and unstrained regions are along the y direction, transverse mode number n will be conserved. Hence $T = \sum_n T_n$ and the problem reduces to solving the 1D Dirac equation. Rescaling by setting $\xi = x/a_0$ yields

$$[-i\sqrt{\Sigma_x(\xi)}\partial_\xi \sqrt{\Sigma_x(\xi)} + \Sigma_y a_0 q_n + v(\xi)]\psi_n(\xi) = \mathcal{E}\psi_n(\xi). \quad (9)$$

Here $\mathcal{E} = Ea_0/(\hbar v_F) \approx E/(4.0 \text{ eV})$, and $v(\xi)$ is the effective (dimensionless) potential in the ribbon.

The effective potential has one contribution $\phi_{\text{BG}}(x,w)$ from the applied backgate field and one contribution ϕ_D from the deformation potential.[42,43] Recent *ab initio* calculations[44] suggest that the contribution to the effective potential from the deformation potential is approximately $\phi_{\text{D}} = g_0\epsilon$, with $g_0 \approx 3$ eV.

An expression for the effective potential from the backgate is derived in Appendix A for the lowest transverse subband. If one assumes an adiabatic approximation along the ribbon, the resulting effective potential is

$$\phi_{\text{BG}} \approx \frac{\mu}{1 + \alpha \ln \frac{8d(x)}{W}}$$
$$\approx \phi_{\text{BG}}^0 \left(1 + \left[\frac{w(x)}{d_0}\right]\frac{\alpha}{1 + \alpha \ln \frac{8d_0}{W}}\right) = \phi_{\text{BG}}^0 + \delta\phi_{\text{BG}}(x). \quad (10)$$

The correction to ϕ_{BG}^0 is proportional to w and hence to $\sqrt{\epsilon}$. However, for realistic geometries (or if a side gate is used) the prefactor is so small that this term can be omitted and we can take $\phi_{\text{BG}}(x) = \phi_{\text{BG}}^0$ for large d. The constant ϕ_{BG} can be incorporated in E and we are left with a uniform strain-dependent scalar deformation potential $v = g_0 a_0/(\hbar v_F)\epsilon \approx 0.74\epsilon$ in the suspended part of the ribbon (region II) and zero potential in regions I and III [see Fig. 1(b)].

To calculate T Eq. (9) should be solved in the regions I, II, and III [see Fig. 1(b)] and the solutions matched at the interfaces (see also Ref. 45). In a region of constant v and uniform ϵ, the solution with energy $\mathcal{E}$ in band n is

$$\psi_n(x) = A_n e^{ikx}\begin{pmatrix} 1 \\ e^{i\theta_n(k)} \end{pmatrix} + B_n e^{-ikx}\begin{pmatrix} 1 \\ -e^{-i\theta_n(k)} \end{pmatrix}, \quad (11)$$

where $\exp[i\theta_n(k)] = \frac{k+iq_n}{\mathcal{E}-v}$ and $k = +\sqrt{(\mathcal{E}-v)^2 - q_n^2}$.

The matching of wave functions between regions is determined by current conservation.[46] The current operator corresponding to the Hamiltonian in Eq. (9) is $\hat{J}_x = 2v_F \Sigma_x \sigma_x$. Consequently, at the interface between regions I and II, $\sqrt{\Sigma_x^I}\psi_n^I = \sqrt{\Sigma_x^{II}}\psi_n^{II}$. However, the factors $\sqrt{\Sigma_x}$ cancel in the final expression for T_n:

$$T_n(E) = \left(1 + \sin^2\phi_n \left[\frac{\sin\theta_{nI} - \sin\theta_{nII}}{\cos\theta_{nI}\cos\theta_{nII}}\right]^2\right)^{-1}. \quad (12)$$

Here $\phi_n \equiv k_{II}L$, while $\theta_{n(I,II)}$ are the propagation angles for electrons in regions I and II.

In Fig. 3, T is shown for strains $\epsilon = 0.0 - 1.0\%$ as the solid lines. The dashed lines correspond to solving the same problem but omitting the deformation potential. The discrete symbols were obtained numerically using the tight-binding Hamiltonian in Eq. (1) with an added deformation potential using the relation $T = \text{Tr}[\Gamma_L G_C^r \Gamma_R G_c^a]$. Here $G_C^{r,(a)}$ are the retarded (advanced) Green's functions for the ribbon, and $\Gamma_{L,R}$ are self-energies accounting for semi-infinite graphene leads. Also, in the numerical calculation no linearization in strain has been made. As can be seen, for the lowest plateau a transport gap opens up with increasing strain.

From Eq. (12) the sensitivity of the conductance $G \propto T$ to ribbon displacements w can be obtained. For the lowest transverse mode $q = 0$ and for $v_{I,II} = 0$ one finds

$$T_0(\mathcal{E}) = \frac{(\mathcal{E} - v)^2 - a_0^2 k_0^2}{(\mathcal{E} - v)^2 - a_0^2 k_0^2 \cos^2 L/a_0 \sqrt{(\mathcal{E} - v)^2 - k_0^2 a_0^2}}. \quad (13)$$

This dependence of T on ϵ is shown in Fig. 4. Different curves correspond to different backgate bias points, i.e., different values of $E = 0.0, 0.3, \ldots$ eV. From this figure it is clear how for a given strain one may chose a working point E_0 (by gating the structure) such that the slope of the $T(\epsilon)$ curve is maximal. This maximal slope $|\partial T/\partial \epsilon|_{\max}$ then defines the sensitivity.

The smallest sensitivity is obtained for the working point at $E = 0$ [dashed-dotted line in Fig. 4]. A lower bound for the sensitivity can be found by setting $\mathcal{E} = 0$ in Eq. (13) and solving for the maximum magnitude of the slope. This gives $|\partial T/\partial \epsilon|_{\max} \approx 2(L/a_0)$. Hence for a deflection of magnitude w, the relative change in conductance is $\delta G/G = \delta T/T \sim w^2/(La_0)$.

In Fig. 4 the dashed lines show the effect of taking into account the change in carrier density due to the deflection-dependent part of the potential $\delta\phi_{\text{BG}}(x)$ in Eq. (10). The calculation was done for a suspension height of $d_0 = 100$ nm. As can be seen, for a short and narrow ribbon the effect of $\delta\phi_{\text{BG}}$ is very small.

This result is valid for a metallic armchair ribbon where all edges are perfect and impurities absent. For transport restricted to the lowest transverse subband, long-range impurity scatterers will not affect the transport.[47] However, short-range potentials will have an effect. For armchair graphene nanoribbons both theory[48] and subsequent experiments[49,50] suggest that at low temperature, edge disorder induce localization. In this case, transport at low energies is governed by variable range hopping and is strongly suppressed. Hence schemes relying on a single armchair ribbon require nearly perfect edges.
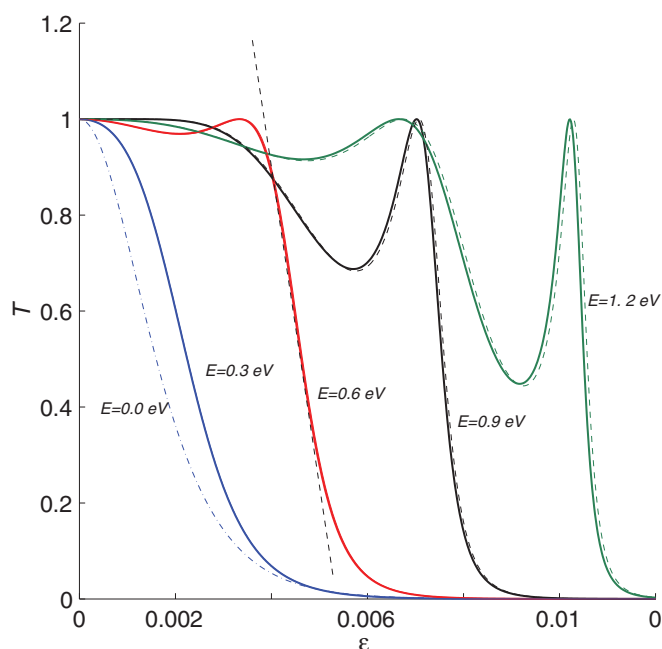

FIG. 4. (Color online) Transmission probability T through a metallic armchair ribbon ($W = 17$ nm, $L = 28$ nm) [see Fig. 1(b)] as a function of strain ϵ. T is shown as function of strain ϵ for energies $E = 0.0, 0.3, 0.6, 0.9, 1.2$ eV. The slope of the straight dashed line determines the sensitivity of the working point around $\epsilon = 0.5\%$. The curved dashed lines show T corrected for displacement-dependent charge density (effective potential) for a ribbon with suspension height $d_0 = 100$ nm.

IV. SUSPENDED ZIGZAG RIBBON INTERFEROMETER

Zigzag nanoribbons are less sensitive to edge disorder. However, applying strain will not lead to a transport gap. Instead, to obtain a sensitivity of $w^2/(La_0)$ an interferometer with the suspended ribbon making up one of the arms [Fig. 1(c)] can be used. The other arm is assumed to rest on the substrate, its strain being unaffected by the backgate. In graphene ring geometries Aharanov-Bohm oscillations have been observed at low temperatures.[51] Here, no external B field is required. Instead, the effective gauge field due to the strain in the suspended arm is exploited.

The idea is again to use the lowest quantized conductance plateau. For zigzag nanoribbons this is formed from current carried by the edge states. Hence consider an edge state coming from the unstrained region I, which split into the two arms IIa and IIb [see Fig. 1(c)]. The state propagating in the strained arm (IIb) will acquire an extra phase $\delta\varphi$ compared to the state propagating in the unstrained arm (IIa). Due to interference, one expects the total transmission to be sensitive to this phase and to modulate the conductance.

In Fig. 5 the result of numerically calculating T (using the tight-binding Hamiltonian) from region I to region III as a function of energy E and strain ϵ is shown. For energies $E < 0.25$ eV, there is only one incoming state from contact I. In this region bright areas correspond to $T = 1$ and dark regions to $T = 0$. For $E > 0.25$ eV there are two incoming modes from region I propagating through the arms. This leads to a total transmission $1 < T < 2$. Below the focus is on the region
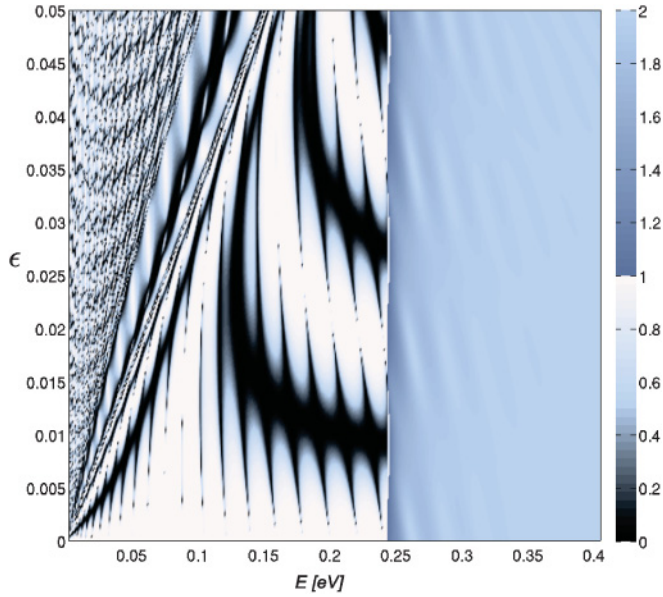
FIG. 5. (Color online) Transmission T as a function of energy E and strain ϵ through the interferometer shown in Fig. 1(c). The figure was generated using the tight-binding Hamiltonian and recursive lattice Green's function on a system of width $W = 2 \times 7.5$ nm, $L = 52$ nm, and a "gap" between the ribbons of 0.5 nm. The broad dark bands can be attributed to destructive interference between states propagating in the two arms. The fine structure is due to backscattering at the point where the ribbon divides into the two arms.

$E < 0.24$ eV, with only a single incoming mode. The alternating broad dark and bright regions in Fig. 5 arise due to interference, whereas the fine structure is the result of backscattering at the interfaces where the ribbon is split.

To reproduce the interference pattern seen in Fig. 5, consider first a zigzag nanoribbon of width W in a constant external potential V and uniform strain strain ϵ. Letting the edge be oriented along the y direction, these propagating states can be found from making the solution Ansatz

$$\Psi(x,y) = e^{iqy}[\Phi(x,q)e^{ik_0 y} + \chi(x,q)e^{-ik_0 y}] \qquad (14)$$

in Eq. (2). Here $\Phi(x,q) = [\Phi_A, \Phi_B, 0, 0]^T$ and $\chi = [0, 0, \phi_A, \phi_B]^T$ are K, K' valley polarized mode wave functions, respectively. As we are interested in transport in one direction only, consider a single valley, the K valley. The boundary conditions on the mode function are $\phi_A(x = 0) = \phi_B(x = W) = 0$, where W is the ribbon width. The (un-normalized) solutions to the resulting eigenvalue equations are

$$\Phi_n(x, q_n) = \begin{pmatrix} \sinh(z_n x) \\ \pm i \sinh(z_n[x - W]) \\ 0 \\ 0 \end{pmatrix}, \qquad (15)$$

where the wave vector q_n and transverse wave number z_n are found from solving the equations

$$q_n = \frac{\Sigma_x z_n}{\Sigma_y \tanh z_n W}, \quad E - V = \pm \frac{\hbar v_F \Sigma_x z_n}{\sinh z_n W}. \qquad (16)$$

For $|E| < \hbar \Sigma_x v_F / W$, $z_n = z_0$ is real, while for $|E| > \hbar \Sigma_x v_F / W$, it is imaginary, $z_n = i \kappa_n$. Similar expressions hold for the K'-valley wave function $\phi_n(x, q_n)$.
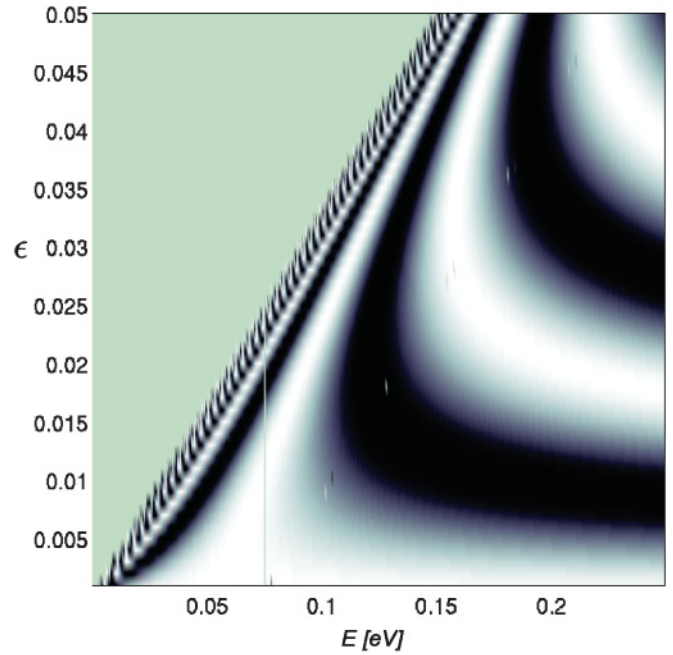

FIG. 6. (Color online) Transmission T as a function of energy E and strain ϵ generated using the expression $(1 + \sin \delta\phi)/2$, where $\delta\phi$ comes from solving Eqs. (16) to obtain the total phase difference $\delta\phi = L(q_a - q_b - k_0)$. The system parameters (length, width, etc.) are the same as for the system in Fig. 5.

Solving Eqs. (16) the wave vectors $q^{(a)}$ and $q^{(b)}$ in the arms IIa and IIb can be found for a given energy E. In the unstrained arm, $q^{(a)}$ is obtained by solving with $\Sigma_x = \Sigma_y = 1$, $V = 0$ whereas in arm IIb, $q^{(b)}$ is found by using $V = g_0 \epsilon$ and $\hat{\Sigma}$ [see Eq. (B3)]. The total phase difference is $\delta\phi = L(q^{(a)} - q^{(b)} - k_0)$, where L is the length of the two interferometer arms and k_0 is given by Eq. (7). When solving Eqs. (16), W is the width of the interferometer arms.

In Fig. 6 the transmission T, calculated as $T = (1 + \sin \delta\phi)/2$, is shown with $\delta\phi$ obtained from solving Eqs. (16). The system parameters (L and W) are the same as for Fig. 5. As can be seen, the agreement is good. For $\epsilon > E/g_0$ no solution is obtained since the Fermi level in the suspended arm is then below the charge neutrality point.

While a general solution of Eqs. (16) requires a numerical treatment, the limit of large energies, where the dispersion is approximately linear, can be solved. In this case $q^{(a)} \approx \pm |E/\hbar v_F|$ and $q^{(b)} \approx \pm |[E - g_0 \epsilon]/\Sigma_y \hbar v_F|$. To first order in ϵ one finds

$$\delta\phi \approx \frac{L}{a_0} \epsilon \left[1.7 + 1.5(E/t_0) - 0.67(g_0/t_0) \right]. \qquad (17)$$

The first term is due to the shift of the Fermi point (synthetic gauge field), whereas the second comes from change of Fermi velocity in the strained region. The last term accounts for the deformation potential. This expression shows that as was the case for the armchair ribbon, one obtains a sensitivity to deflections of $\delta G/G = \delta T/T \sim (w^2/La_0)$.

The effect of edge disorder on the transmission T is shown in Fig. 7. Here, disorder has been accounted for by removing the outermost atoms with probability p at random along each of the four zigzag edges of the interferometer. The same system
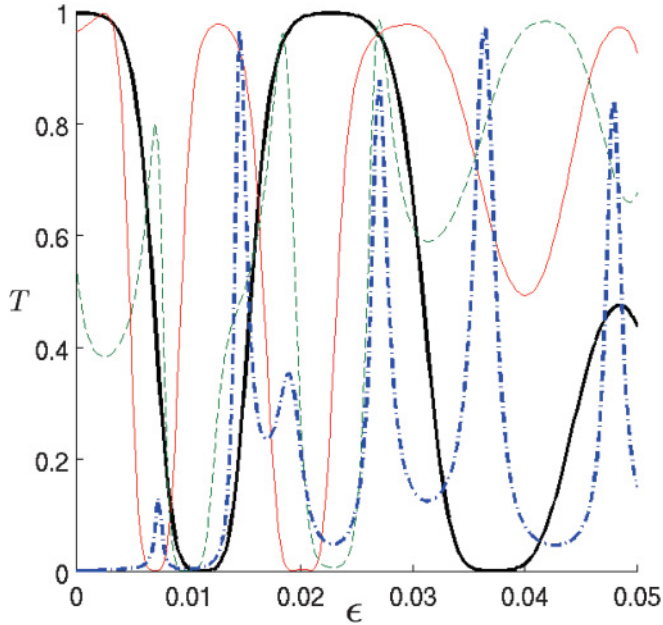
FIG. 7. (Color online) Transmission probability $T(E,\epsilon)$ at constant $E = 0.19$ eV as a function of strain ϵ for varying degrees of edge disorder. The system geometry is the same as that used in Fig. 5. The thick black line is T without disorder whereas the thin lines correspond to removing edge atoms with probability p along the edges. Thin solid red line: $p = 0.1$. Dashed green line: $p = 0.2$. Dash dotted blue line: $p = 0.3$.

as used in Fig. 5 was used and the curves correspond to a constant $E = 0.19$ eV. The thick black line shows $T(\epsilon)$ without disorder, whereas the other curves (see figure caption) show the transmission for $p = 0.1, 0.2, 0.3$. While the presence of the disorder distorts the interference pattern, clear conductance modulations with the same amplitude variation and magnitude of $|\partial T/\partial \epsilon|$ as in the absence of disorder can be seen. For stronger disorder, conductance fluctuations with changing strain is still seen but the overall transmission is suppressed.

For a more generic boundary which is not aligned exactly along the zigzag edge, the sensitivity is expected to be of the same order of magnitude. As shown in Ref. 52, a ribbon with a generic boundary typically displays the characteristics of a zigzag ribbon. As the shift of **k** is always along the (proper) zigzag direction, the phase shift giving rise to interference will be smaller. This will increase the relative importance of the phase gained from, for instance, the deformation potential and the Fermi velocity renormalization in Eq. (17).

V. CONCLUSIONS

In conclusion, by exploiting the possibility to directly integrate coherent electron transport with graphene nanoribbon NEMS, the conductance through the structure can be made to depend on the mechanical deflection w as $\delta G/G \sim (w^2)/(La_0)$. For a single armchair ribbon this is mainly due to the strain-induced shift of the Fermi points (synthetic gauge field) and the associated transport gap. For the zigzag interferometer-type setup it is the result of a combination of synthetic gauge field, the renormalized Fermi velocity, as well as the deformation potential.

APPENDIX A: ELECTROSTATICS OF SUSPENDED RIBBONS

Consider first a simple mean field estimate of the effect of charging energy in a nanoribbon. Hence the nanoribbon is treated as a perfect conductor of width W suspended a distance d above a backgate. If $W/d \ll 1$ the electrostatic potential ϕ on the surface of the conductor is related to its 1D charge density through[53,54]

$$\phi \approx \frac{\rho}{2\pi\epsilon_0} \ln \frac{8d}{W} + \mathcal{O}(W/d).$$

For a ribbon connected to a reservoir at chemical potential μ, this implies that to account for charging energy the bare chemical potential μ should be replaced by an effective chemical potential $v_{\text{eff}} = \mu - e\phi/2$.

In the lowest transverse subband of a nanoribbon, the 1D charge density is proportional to v_{eff} and is given by

$$\rho = \frac{4}{3\pi t_0 a_0} v_{\text{eff}}.$$

From this one finds the relation between chemical potential (backgate bias) and the effective chemical potential

$$v_{\text{eff}} \approx \kappa\mu = \frac{\mu}{1 + \frac{e^2}{3\pi^2 t_0 a_0 \epsilon_0} \ln \frac{8d}{W}}. \tag{A1}$$

In deriving Eq. (A1), the graphene strip was assumed to behave as a macroscopic metallic strip. For a narrow wire, quantum effects may become important. To obtain an approximate validation of Eq. (A1) it was compared to numerical solutions of the tight-binding Hamiltonian in the presence of Coulomb interactions. The interactions were treated in the self-consistent Hartree approximation along the lines of Ref. 55. The results are shown as the open circles in Fig. 8. The circles were obtained for solving for widths between $1.2 < W < 10$ nm and heights $10 < d < 100$ nm. As can be seen, for the heights and widths considered, Eq. (A1) yields a reasonable approximation.

APPENDIX B: DEFLECTION OF SUSPENDED RIBBONS

The stationary mechanical deformation of a suspended graphene sheet subject to an external pressure in the direction normal to the surface is determined by the von-Karman equations for thin plates.[24] Following Ref. 56 and considering an underformed graphene sheet in the xy plane subject to a pressure P, the differential equations may be written as (see Sec. 14 in Ref. 56)

$$\kappa\Delta^2 w - \frac{\partial}{\partial x}\left[\sigma_{xx}\frac{\partial w}{\partial x} + \sigma_{yx}\frac{\partial w}{\partial y}\right]$$
$$- \frac{\partial}{\partial y}\left[\sigma_{xy}\frac{\partial w}{\partial x} + \sigma_{yy}\frac{\partial w}{\partial y}\right] = P, \tag{B1}$$
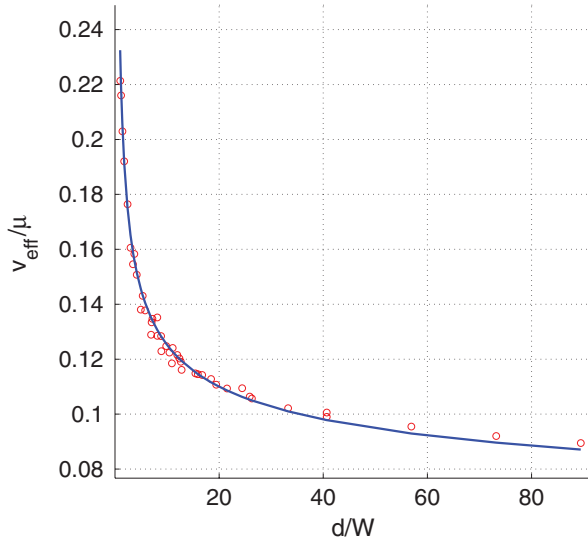
FIG. 8. (Color online) Comparison between quantum mechanical simulation in self-consistent Hartree approximation and analytical estimates for narrow armchair ribbons with only the lowest transverse subband occupied. Shown is the constant of proportionality between reservoir chemical potential μ and effective chemical potential $v_{\rm eff}$ in the ribbon due to electron-electron interactions. The solid lines represent Eq. (A1), while the circles come from solving the the Schrodinger equation self-consistently.

where to ensure equilibrium the condition

$$\frac{\partial \sigma_{xx}}{\partial x} + \frac{\partial \sigma_{xy}}{\partial y} = \frac{\partial \sigma_{yx}}{\partial x} + \frac{\partial \sigma_{yy}}{\partial y} = 0 \qquad \text{(B2)}$$

must be fulfilled. Here the notation (u, v, w) is used to denote the Cartesian components of the displacement vector. As graphene is an intrinsic two-dimensional material, the stress tensor σ_{ij} has here units of Nm^{-1} and the bending rigidity $\kappa \approx 1$ eV is the intrinsic bending rigidity of graphene.

The stress tensor is determined from the strain tensor, and in terms of the displacement vector one finds

$$\sigma_{xx} = (\lambda + 2\mu)\left(\frac{\partial u}{\partial x} + \frac{1}{2}|\nabla w|^2\right) + \lambda \frac{\partial v}{\partial y} - \mu \left(\frac{\partial w}{\partial y}\right)^2,$$

$$\sigma_{yy} = (\lambda + 2\mu)\left(\frac{\partial v}{\partial y} + \frac{1}{2}|\nabla w|^2\right) + \lambda \frac{\partial u}{\partial x} - \mu \left(\frac{\partial w}{\partial x}\right)^2, \quad \text{(B3)}$$

$$\sigma_{xy} = \mu \left(\frac{\partial v}{\partial x} + \frac{\partial u}{\partial y} + \frac{\partial w}{\partial x}\frac{\partial w}{\partial y}\right).$$

Here $\mu \approx 3\lambda \approx 9$ eV/Å^2 are the Lame coefficients of graphene and $\lambda + 2\mu \approx 340$ N/m.[57] For any given pressure $P(x, y)$ the static deflection can be found from solving Eqs. (B1), (B2), and (B3).

For a narrow graphene ribbon one may simplify the equations by making the assumption that the deflection w and

the strains σ_{ij} are constant across the ribbon, i.e., $w(x, y) = w(x)$ and $\sigma_{ij}(x, y) = \sigma_{ij}(x)$. This leads to the equations for a thin beam

$$\kappa \Delta^2 w - T_x \frac{\partial^2 w}{\partial x} = P, \qquad \text{(B4)}$$

where $T_x = \sigma_{xx} + T_0$ is a constant tension in the ribbon, with σ_{xx} given by

$$\sigma_{xx} = \frac{\lambda + 2\mu}{2L} \int_0^L dx \left(\frac{\partial w}{\partial x}\right)^2. \qquad \text{(B5)}$$

The built-in tension $T_0 = (\lambda + 2\mu)\epsilon_x^0$ has here been added to the tension σ_{xx} arising from the deflection. This tension arises typically in suspended graphene, as they tend to have the shape shown in Fig. 2 with a net strain $\epsilon_x^0 > 0$ in the suspended part. As any large curvature occurs only in the immediate vicinity of the point of attachment to the electrode, this taken together with the smallness of κ implies that for the subsequent analysis of the deformation the first term $\kappa \partial^4 w / \partial x^4$ can be dropped.[24]

Solving Eqs. (B4) and (B5) for constant P with boundary conditions $w(0) = w(L) = 0$ and $\kappa = 0$ then yields

$$w(x) = -\frac{PL^2}{2T_x}\left[\left(\frac{x}{L}\right)^2 - \frac{x}{L}\right], \qquad \text{(B6)}$$

where T_x is found from solving $T_x = (\lambda + 2\mu)[\epsilon_x^0 + P^2 L^2 / (24 T_x^2)]$.

To estimate the maximum deflection for a given P, consider the case with no built-in strain in the x direction ($\epsilon_x^0 = 0$). This gives a maximum deflection of

$$w_{\rm max} = \frac{L}{4}\left(\frac{3PL}{\lambda + 2\mu}\right)^{1/3}. \qquad \text{(B7)}$$

On the other hand, if the built-in strain ϵ_{0x} dominates σ_{xx} can be ignored and one finds

$$w_{\rm max} = \frac{P_z L^2}{8\epsilon_x^0 (\lambda + 2\mu)}. \qquad \text{(B8)}$$

For an applied pressure $P_z = e^2/(8\pi \epsilon_0 W^3 d)$ corresponding to $\rho = \rho_{\rm max} \sim e/W$, Eq. (B8) shows that a built-in strain of $\epsilon_0 \approx 0.5\%$ results in a maximum deflection of $w_{\rm max} \approx 10^{-2}(\frac{L}{W})^2 \frac{1}{Wd}$ nm, where W, d, and L are all measured in nanometers. Hence for a geometry with $d = 100$ nm, $L = 100$ nm, and $W = 10$ nm the maximum deflection due to charging will be less than 10^{-3} nm, which can safely be neglected.

However, if the built-in tension approaches zero, i.e., $\epsilon_x^0 = 0$, one must apply Eq. (B7) instead. Then the maximum deflection for the same geometry becomes larger with $w_{\rm max} \approx 3 \times 10^{-2}(\frac{L}{W})(\frac{L}{d})^{1/3} \approx 0.3$ nm. In this case, $w_{\rm max}$ is so large that one must either increase d_0 or circumvent the problem by using a side gate rather than a backgate to control the charge density.

---

* andreas.isacsson@chalmers.se

[1] K. L. Ekinci and M. L. Roukes, Rev. Sci. Instrum. **76**, 061101 (2005).

[2] C. T. C. Nguyen, in *Solid-State Device Research Conference 2006, ESSDERC 2006, Proceedings of the 36th European Conference* (IEEE, 2006), pp. 7–16.

[3] A. Boisen, Nat. Nanotechnol. **4**, 404 (2009).

[4] J. Atalaya, A. Isacsson, and J. M. Kinaret, Europhys. Lett. **91**, 48001 (2010).

[5] M. Blencowe, Phys. Rep. **395**, 159 (2004).

[6] K. C. Schwab and M. L. Roukes, Phys. Today **58**(7), 36 (2005).

[7] A. D. O'Connell, M. Hofheinz, M. Ansmann, R. C. Bialczak, M. Lenander, E. Lucero, M. Neeley, D. Sank, H. Wang, M. Weides, J. Wenner, J. M. Martinis, and A. N. Cleland, Nature **464**, 697 (2010).

[8] K. L. Ekinci, Small **1**, 786 (2005).

[9] J. S. Bunch, A. M. van der Zande, S. S. Verbridge, I. W. Frank, D. M. Tanenbaum, J. M. Parpia, H. G. Craighead, and P. L. McEuen, Science **315**, 490 (2007).

[10] D. Garcia-Sanchez, A. M. van der Zande, A. San Paulo, B. Lassagne, P. L. McEuen, and A. Bachtold, Nano Lett. **8**, 1399 (2008).

[11] J. T. Robinson, M. Zalalutdinov, J. W. Baldwin, E. S. Snow, Z. Wei, P. Sheehan, and B. H. Houston, Nano Lett. **8**, 3441 (2008).

[12] J. S. Bunch, S. S. Verbridge, J. S. Alden, A. M. van der Zande, J. M. Parpia, H. G. Craighead, and P. L. McEuen, Nano Lett. **8**, 2458 (2008).

[13] C. Chen, S. Rosenblatt, K. I. Bolotin, W. Kalb, P. Kim, I. Kymissis, H. L. Stormer, T. F. Heinz, and J. Hone, Nat. Nanotechnol. **4**, 861 (2009).

[14] V. Singh, S. Sengupta, H. S. Solanki, R. Dhall, A. Allain, S. Dhara, P. Pant, and M. M. Deshmukh, Nanotechnology **21**, 165204 (2010).

[15] A. M. van der Zande, R. A. Barton, J. S. Alden, C. S. Ruiz-Vargas, W. S. Whitney, P. H. Q. Pham, J. Park, J. M. Parpia, H. G. Craighead, and P. L. McEuen, Nano Lett. **10**, 4869 (2010).

[16] Y. Xu, C. Chen, V. V. Deshpande, F. A. DiRenno, A. Gondarenko, D. B. Heinz, S. Liu, P. Kim, and J. Hone, Appl. Phys. Lett. **97**, 243111 (2010).

[17] C. Berger, Z. Song, X. Li, X. Wu, N. Brown, C. Naud, D. Mayou, T. Li, J. Hass, A. N. Marchenkov, E. H. Conrad, P. N. First, and W. A. de Heer, Science **312**, 1191 (2006).

[18] H. B. Heersche, P. Jarillo-Herrero, J. B. Oostinga, L. M. K. Vandersypen, and A. F. Morpurgo, Nature **446**, 56 (2007).

[19] M. Huefner, F. Molitor, A. Jacobsen, A. Pioda, C. Stampfer, K. Ensslin, and T. Ihn, New J. Phys. **12**, 043054 (2010).

[20] K. I. Bolotin, K. J. Sikes, Z. Jiang, M. Klima, G. Fudenberg, J. Hone, P. Kim, and H. L. Stormer, Solid State Commun. **146**, 351 (2008).

[21] X. Du, I. Skachko, A. Barker, and E. Y. Andrei, Nat. Nanotechnol. **3**, 491 (2008).

[22] S. Adam and S. Das Sarma, Solid State Commun. **146**, 356 (2008).

[23] M. V. Medvedyeva and Ya. M. Blanter, Phys. Rev. B **83**, 045426 (2011).

[24] J. Atalaya, A. Isacsson, and J. M. Kinaret, Nano. Lett. **8**, (2008).

[25] A. H. Castro Neto, F. Guinea, N. M. R. Peres, K. S. Novoselov, and A. K. Geim, Rev. Mod. Phys. **81**, 109 (2009).

[26] Y. Lee, S. Bae, H. Jang, S. Jang, S.-E. Zhu, S. H. Sim, Y. I. Song, B. H. Hong, and J.-H. Ahn, Nano Lett. **10**, 490 (2010).

[27] Y.-M. Lin, V. Perebeinos, Z. Chen, and P. Avouris, Phys. Rev. B **78**, 161409 (2008).

[28] C. Lian, K. Tahy, T. Fang, G. Li, H. G. Xing, and D. Jena, Appl. Phys. Lett. **96**, 103109 (2010).

[29] N. Tombros, A. Veligura, J. Junesch, M. H. D. Guimarães, I. J. V.-Marun, H. T. Jonkman, and B. J. van Wees, Nat. Phys. **7**, 697 (2011).

[30] M. M. Fogler, F. Guinea, and M. I. Katsnelson, Phys. Rev. Lett. **101**, 226804 (2008).

[31] V. M. Pereira and A. H. Castro Neto, Phys. Rev. Lett. **103**, 046801 (2009).

[32] E. Prada, P. San-Jose, G. Leon, M. M. Fogler, and F. Guinea, Phys. Rev. B **81**, 161402(R) (2010).

[33] F. von Oppen, F. Guinea, and E. Mariani, Phys. Rev. B **80**, 075420 (2009).

[34] Y. Zhang, G. Yu, and J. Dong, Phys. Rev. B **73**, 205419 (2006).

[35] A. Maiti, A. Svizhenko, and M. P. Anantram, Phys. Rev. Lett. **88**, 126805 (2002).

[36] C. L. Kane and E. J. Mele, Phys. Rev. Lett. **78**, 1932 (1997).

[37] P. E. Lammert and V. H. Crespi, Phys. Rev. B **61**, 7308 (2000).

[38] L. Yang and J. Han, Phys. Rev. Lett. **85**, 154 (2000).

[39] A. Kleiner and S. Eggert, Phys. Rev. B **63**, 073408 (2001).

[40] L. Sun, Q. Li, H. Ren, H. Su, Q. W. Shi, and J. Yang, J. Chem. Phys. **129**, 074704 (2008).

[41] R. M. Ribeiro, V. M. Pereira, N. M. R. Peres, P. R. Briddon, and A. H. Castro Neto, New J. Phys. **11**, 115002 (2009).

[42] J. Bardeen and W. Shockley, Phys. Rev. **80**, 72 (1950).

[43] H. Suzuura and T. Ando, Phys. Rev. B **65**, 235412 (2002).

[44] S.-M. Choi, S.-H. Jhi, and Y.-W. Son, Phys. Rev. B **81**, 081407(R) (2010).

[45] N. M. R. Peres, Rev. Mod. Phys. **82**, 2673 (2010).

[46] A. V. Kolesnikov and A. P. Silin, Zh. Eksp. Teor. Fiz. **109**, 2125 (1996) [JETP **82**, 1146 (1996)].

[47] M. Yamamoto, Y. Takane, and K. Wakabayashi, Phys. Rev. B **79**, 125421 (2009).

[48] I. Martin and Ya. M. Blanter, Phys. Rev. B **79**, 235132 (2009).

[49] M. Y. Han, J. C. Brant, and P. Kim, Phys. Rev. Lett. **104**, 056801 (2010).

[50] R. Danneau, F. Wu, M. Y. Tomi, J. B. Oostinga, A. F. Morpurgo, and P. J. Hakonen, Phys. Rev. B **82**, 161405(R) (2010).

[51] S. Russo, J. B. Oostinga, D. Wehenkel, H. B. Heersche, S. S. Sobhani, L. M. K. Vandersypen, and A. F. Morpurgo, Phys. Rev. B **77**, 085413 (2008).

[52] A. R. Akhmerov and C. W. J. Beenakker, Phys. Rev. B **77**, 085423 (2008).

[53] W. R. Smythe, *Static and dynamic electricity* (McGraw-Hill, New York, 1968).

[54] P. G. Silvestrov and K. B. Efetov, Phys. Rev. B **77**, 155436 (2008).

[55] J. Fernandez-Rossier, J. J. Palacios, and L. Brey, Phys. Rev. B **75**, 205441 (2007).

[56] L. D. Landau and E. M. Lifshitz, *Theory of Elasticity* (Pergamon, Oxford, 1986).

[57] K. N. Kudin, G. E. Scuseria, and B. I. Yakobson, Phys. Rev. B **64**, 235406 (2001).